Precise Orbit Determination of the ZY3-03 Satellite Using the Yaw-Attitude Modeling for Drift Angle Compensation

Xuewen Gong, Wanke Liu, Fuhong Wang, Qingpeng Li, Jingmei Li, Xueli Chang, and Shuaihe Gao

***Abstract*—The ZY3-03 satellite exhibits a special yaw-steering state to compensate for the drift angle of onboard space cameras with the time-delay-and-integration charge-coupled devices (TDICCDs). The commonly used zero-attitude model, which assumes zero yaw, pitch, and roll angles, is no longer suitable. A targeted yaw-attitude model is proposed to express this special yaw state. It still defaults zero pitch and roll angles, but calculates the drift angle based on the orbit of the satellite first, and then adopts the opposite of the drift angle as the yaw angle. The orbit determination experiments have revealed that the zero-yaw assumption in the zero-attitude model would result in periodic orbit errors of up to ±86 mm in the normal direction, while the proposed model can describe yaw angle variations accurately with errors of less than ±0.01° in most epochs, and thus avoid the significant normal orbit errors. The proposed yaw-attitude model contributes to the higher precision orbit determination of ZY3-03. Furthermore, this yaw-attitude model also holds practical value for achieving higher precision orbit determination of other remote sensing satellites similar to ZY3-03, especially when the measured attitude data are not available.**

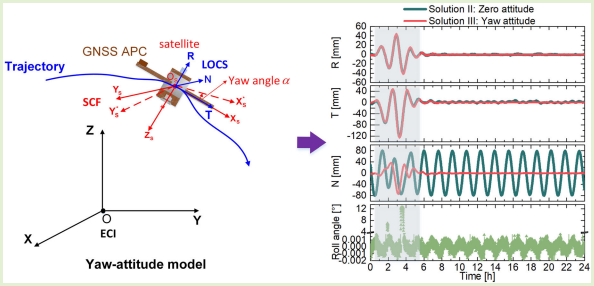

***Index Terms*— Drift angle, orbit determination, yaw-attitude model.**

I. Introduction

ACCURATE and reliable orbit information of remote sensing satellites is essential for spaceborne Earth observation systems. Since America's global positioning system (GPS) was applied for the precise orbit determination (POD) of the Landsat-4 satellite in the 1980s [1], global navigation satellite system (GNSS), including GPS, Russia's global navigation satellite system (GLONASS), and the later Europe's Galileo navigation satellite system (Galileo) and China's BeiDou navigation satellite system (BDS), has gradually become one of the most mainstream POD techniques for the remote sensing satellites on low Earth orbits (LEO) nowadays [2], [3], [4], [5], [6], [7], [8]. For any remote sensing satellite equipped with a GNSS receiver, GNSS signals of various frequencies could be tracked by the receiver with global coverage, and a large quantity of redundant and high-precision GNSS observations could be generated. GNSS measurements and the force models acting on the satellite are integrated to estimate the orbit parameters, easily achieving precise orbits at the centimeter level [8], [9], [10], [11], [12].

Extensive previous studies have demonstrated that satellite attitude is a critical factor affecting the accuracy of POD [2], [13], [14], [15]. On one hand, nonconservative forces, including atmospheric drag, solar radiation pressure, and Earth radiation pressure, typically require satellite panel modeling, necessitating the input of satellite attitude. On the other hand, the antenna phase center (APC) of the GNSS receiver, which is the actual point of GNSS signal reception, does not align with the center of mass (CoM) of the satellite—the acting point of force models and final orbit output—making the transformation from APC to CoM crucial for POD processing. Naturally, transformation errors are

Manuscript received 7 April 2024; accepted 30 May 2024. Date of publication 10 June 2024; date of current version 1 August 2024. This work was supported in part by the National Key Research and Development Program of China under Grant 2023YFB3906500; in part by the National Natural Science Foundation of China under Grant 42304030, Grant 62103307, and Grant 12273045; in part by the State Key Laboratory of Satellite Navigation System and Equipment Technology, Shijiazhuang, Hebei, China, under Grant CEPNT-2021KF-10. The associate editor coordinating the review of this article and approving it for publication was Dr. Hassen Fourati. *(Corresponding author: Xuewen Gong.)*

Xuewen Gong and Shuaihe Gao are with the National Time Service Center and Key Laboratory of Time Reference and Applications, Chinese Academy of Sciences, Xi'an 710600, China (e-mail: gongxuewen@ntsc.ac.cn; gaoshuaihe@nstc.ac.cn).

Wanke Liu and Fuhong Wang are with the School of Geodesy and Geomatics, Wuhan University, Wuhan 430079, China (e-mail: wkliu@sgg.whu.edu.cn; fhwang@sgg.whu.edu.cn).

Qingpeng Li is with China Centre for Resources Satellite Data and Application, Beijing 100094, China (e-mail: 626172666@qq.com).

Jingmei Li is with Aerospace Information Research Institute, Chinese Academy of Sciences, Beijing 100094, China (e-mail: lijm@aircas.ac.cn).

Xueli Chang is with the School of Computer Science, Hubei University of Technology, Wuhan 430068, China (e-mail: chang99@hbut.edu.cn).

Digital Object Identifier 10.1109/JSEN.2024.3409027

significantly impacted by errors in satellite attitude. Remote sensing satellites commonly carry relevant payloads such as star sensors, gyroscopes, infrared sensors, and horizon sensors to measure precise attitudes directly. However, measured attitude data may not always be available for POD due to some factors such as untimely data transmission, equipment failure, or data confidentiality. Thus, when measured attitude data are unavailable, relevant attitude models should be constructed to describe attitude variations in POD processing.

Unlike various geodetic or telecommunication satellites for which a zero-attitude mode is widely used, the attitude mode of remote sensing satellites usually presents different situation in practice. Many remote sensing satellites use the time-delay-and-integration charge-coupled devices (TDICCDs) for the push-broom mode of onboard space cameras. Factors such as orbital motion, satellite attitude variation, and Earth's rotation can lead to a drift angle between the push-broom direction and the target motion direction on the image plane [16]. The drift angle can cause a lateral image shift that is perpendicular to the push-broom direction. This shift can lead to a drop in the modulation transfer function (MTF) and a decrease in image quality [17], [18], [19]. To prevent the negative impact of the drift angle on the image, compensating for it beforehand is essential. There are typically two compensation methods for the drift angle. One is to rotate the focal plane through camera mechanisms [20], [21]. The other is to adjust the satellite yaw angle in the opposite direction of the drift angle, thus ensuring the push-broom direction consistent with the target motion direction [22], [23]. The latter method has been widely used in many remote sensing missions, such as China's Gaofen and ZiYuan (ZY) series and GouMang satellites. This countermeasure for the drift angle can result in a special yaw-steering state for the satellite. When the measured satellite attitude is unavailable, it is crucial to construct a yaw-attitude model to describe this unique state in high-precision POD processing. However, this issue seems to be rarely mentioned in previous POD studies. This negligence may be attributed to two factors. First, the measured attitude data are often available, making it unnecessary to develop a yaw-attitude model most of the time. Second, this special yaw-attitude caused by the TDICCD space cameras has not been widely realized by POD researchers, even though remote sensing researchers know it well.

To address this gap, we aim to construct a corresponding yaw-attitude model to describe the special yaw-steering state and conduct an in-depth study of GNSS-based POD with this model. The ZY3-03 satellite, manufactured by the China Academy of Space Technology and launched on July 25, 2020, is a typical remote sensing satellite that carries the TDICCD space camera and compensates for the drift angle through yaw control [24]. The satellite flies on a sun-synchronous orbit with an altitude of about 505 km and an inclination of about 97.4°. More importantly, the ZY3-03 satellite is equipped with a dual-frequency GPS receiver, start sensor and laser reflector, which provide dual-frequency (L1+L2) GPS measurements, precise measured attitude data, and satellite laser ranging (SLR) data, respectively, so the GPS-based POD experiments of ZY3-03 could be conducted and assessed conveniently to validate the effectiveness of the constructed yaw-attitude model. Therefore, the ZY3-03 satellite will be taken as the research target in this contribution. The research is significant for promoting higher precision POD processing of remote sensing satellites.

The following text will introduce the computation method of the drift angle and present the yaw-attitude model for drift angle compensation in detail, comparing it to the commonly used zero-attitude model. Meanwhile, the influences of attitude model errors on the POD will be analyzed based on detailed formula derivation. Then, taking the ZY3-03 satellite as the target, attitude error analyses are conducted using measured attitude data as a reference for both the attitude models. A series of ZY3-03 POD experiments based on onboard GPS data will be performed and compared among the zero-attitude model, the yaw-attitude model, and the measured attitude data to validate the effectiveness of the proposed yaw-attitude model. Finally, the study will be concluded.

II. Yaw-Attitude Modeling

The attitude model and the measured attitude data are used to describe the relationship between the spacecraft-fixed coordinate system (SCS) and a space coordinate system, such as the commonly used Earth-centered inertial (ECI) system. While measured attitude data can provide the measured rotation matrix, rotation Euler angle, or quaternions between SCS and ECI at each epoch, the attitude model establishes an analytical formula for transforming the two coordinate systems. Taking into account the fact that the special yaw-steering state of the ZY3-03 satellite is to compensate for the drift angle of the TDICCD space camera, the first step of yaw-attitude modeling is to compute the drift angle. With the drift angle known, the yaw state can be achieved, and then the yaw-attitude model can be established.

A. Drift Angle

The drift angle of the TDICCD space camera is closely related to the pitch and roll attitudes of the satellite platform [25]. For the ZY3-03 satellite, the pitch and roll angles typically vary irregularly and can only be obtained based on measured attitude data. However, if the measured attitude data are already available, the yaw-attitude of the satellite can be obtained directly. In this case, there is no need to compute the drift angle to determine the yaw state of the satellite. Therefore, for POD processing, only the computation formula of the drift angle, without considering the effects of roll and pitch attitudes, is feasible and necessary when measured attitude data are unavailable. This means that the calculation of the drift angle should only be performed in cases where the pitch and roll angles are zero. Regarding the pitch and roll angles of the satellite as zero, Fig. 1 shows relevant geometric relationships in the computation of drift angle. Under the ECI system $O-\mathbf{XYZ}$, setting the position and velocity of the satellite as $(\boldsymbol{r}, \boldsymbol{v})$ at a certain epoch, point S represents the subsatellite point, namely, the imaging point, and point N represents the ascending node. Taking point O as the origin to draw a big circle through axis $\mathbf{Z}$ and point S, the circle intersects with plane $O-\mathbf{XY}$ at point D.

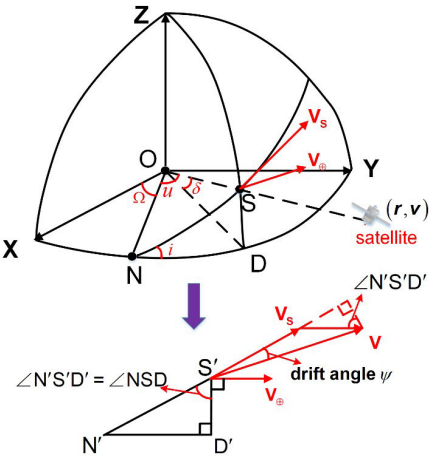

Fig. 1. Geometric relationship for the computation of drift angle; $\Delta N'S'D'$ is a forward projection of the spherical right triangle ΔNSD in the plane perpendicular to the vector **OS** at the imaging point S.

According to the geometric relationship in Fig. 1 and relevant descriptions in [25], the drift angle could be computed as follows.

1) First, six Kepler orbit elements, namely the semi-major axis a, the eccentricity e, the right ascension of the ascending node Ω, the orbital inclination i, the argument of perigee ω, and the mean anomaly M, are computed based on the position and velocity $(\boldsymbol{r}, \boldsymbol{v})$ of the satellite under ECI.
2) Second, the eccentric anomaly E, the true anomaly υ, and the argument of latitude u could be computed successively, and then the declination δ of the imaging point S and the angle $\angle$NSD of the spherical right triangle ΔNSD are achieved based on the following formula:

$$\begin{cases} E = M + e\sin E;\ \upsilon = \arctan\left(\dfrac{\sqrt{1-e^2}\sin E}{\cos E - e}\right) \\ u = \upsilon + \omega \\ \delta = \arcsin\left(\sin i \cdot \sin u\right);\ \angle\text{NSD}=\arccos\left(\tan\delta \cdot \cot u\right). \end{cases} \tag{1}$$

3) $\mathbf{V_S}$ and $\mathbf{V}_\oplus$ represent the traction velocities of the imaging point S caused by the satellite motion and the Earth's rotation, respectively, so the overall traction velocity of S should be $\mathbf{V} = \mathbf{V_S} + \mathbf{V}_\oplus$. The angle between $\mathbf{V_S}$ and $\mathbf{V}$ is defined as the drift angle ψ. According to the geometric relationship in Fig. 1, the computation formula is as follows:

$$\begin{cases} |\mathbf{V}_\oplus| = \omega_\oplus \cdot r_\oplus \cdot \cos\delta;\ |\mathbf{V_S}| = \sqrt{\dfrac{\mu}{a^3}} \cdot r_\oplus \\ \psi = \arctan\left(\dfrac{|\mathbf{V}_\oplus| \cdot \cos\left(\angle\text{NSD}\right)}{|\mathbf{V_S}| + |\mathbf{V}_\oplus| \cdot \sin\left(\angle\text{NSD}\right)}\right) \end{cases} \tag{2}$$

where $r_\oplus, \omega_\oplus$, and μ denote the radius, the rotation angular velocity, and the gravitational constant of the Earth, respectively.

B. Yaw-Attitude Model

Before delving into yaw-attitude modeling, it is essential to first elaborate on a very common zero-attitude model, which is widely used for many geodetic or telecommunication satellites. Essentially, the yaw state of the ZY3-03 satellite is to perform a certain rotation about the yaw axis based on this zero attitude. A local orbital coordinate system (LOCS) $O_S - \mathbf{RTN}$ is established first in Fig. 2, where O_S represents the CoM of the satellite, the radial (R) axis $\mathbf{R}$ points from the geocentric to the satellite, the tangential (T) axis $\mathbf{T}$ points to the flight direction, and the normal (N) axis $\mathbf{N}$ forms a right-handed rectangular system with them $(\mathbf{N} = \mathbf{R} \times \mathbf{T})$. The yaw, roll, and pitch angles of the satellite platform are usually defined as three rotation angles between SCS $O_S - \mathbf{X_S Y_S Z_S}$ and a middle coordinate system $O_S - \mathbf{T}\,(-\mathbf{N})\,(-\mathbf{R})$ which is obtained from a simple conversion of LOCS $O_S - \mathbf{RTN}$. Just as its name implies, the zero-attitude model defaults the yaw, roll, and pitch angles as zero. It is equivalent to that the axes $\mathbf{X_S}$, $\mathbf{Y_S}$, and $\mathbf{Z_S}$ of SCS are defined as parallel positively to the axes $\mathbf{T}$, $-\mathbf{N}$, and $-\mathbf{R}$, respectively. Therefore, the analytical formula of the zero-attitude could be set up to describe the relationships between SCS $O_S - \mathbf{X_S Y_S Z_S}$, ECI $O - \mathbf{XYZ}$. and LOCS $O_S - \mathbf{RTN}$, as follows:

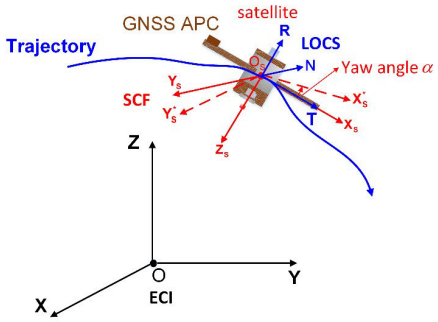

Fig. 2. Geometric relationship between different coordinate systems; $O - \mathbf{XYZ}$, $O_S - \mathbf{X_S Y_S Z_S}$, and $O_S - \mathbf{RTN}$ represent the ECI system, the SCS, and the LOCS, respectively; $O_S - \mathbf{X_S^* Y_S^* Z_S^*}$ represents the SCS after yaw rotation.

$$\begin{cases} [\text{ECI}] = \begin{bmatrix} \mathbf{e}_R & \mathbf{e}_T & \mathbf{e}_N \end{bmatrix} \cdot [\text{LOCS}] \\ [\text{LOCS}] = \begin{bmatrix} 0 & 0 & -1 \\ 1 & 0 & 0 \\ 0 & -1 & 0 \end{bmatrix} \cdot [\text{SCS}] \\ [ECI] = \begin{bmatrix} e_T & -e_N & -e_R \end{bmatrix} \cdot [\text{SCS}] \end{cases}, \text{where} \begin{cases} \mathbf{e}_R = \dfrac{\boldsymbol{r}}{|\boldsymbol{r}|} \\ \mathbf{e}_N = \dfrac{\boldsymbol{r} \times \boldsymbol{v}}{|\boldsymbol{r} \times \boldsymbol{v}|} \\ \mathbf{e}_T = \mathbf{e}_N \times \mathbf{e}_R \end{cases} \tag{3}$$

where, $\mathbf{e}_R$, $\mathbf{e}_T$, and $\mathbf{e}_N$ denote the unit vectors of the $\mathbf{R}$, $\mathbf{T}$, and $\mathbf{N}$ axes under ECI, respectively.

The ZY3-03 satellite aims to compensate for the drift angle of the TDICCD space camera through yaw control, the original SCS $O_S - \mathbf{X_S Y_S Z_S}$ of the satellite must undergo a certain yaw angle to the new SCS $O_S - \mathbf{X_S^* Y_S^* Z_S^*}$, and the yaw angle α should be equal to the drift angle ψ but in the opposite direction, i.e., $\alpha = -\psi$. Under this circumstance, the zero-attitude model mentioned above can no longer describe the relationship between the new SCS $O_S - \mathbf{X_S^* Y_S^* Z_S^*}$, LOCS $O_S - \mathbf{RTN}$, and ECI $O - \mathbf{XYZ}$. At this time, the analytical formula for the yaw-attitude model can be established as

follows:

$$\begin{cases} [\text{ECI}] = \begin{bmatrix} e_R & e_T & e_N \end{bmatrix} \cdot [\text{LOCS}] \\ [\text{LOCS}] = \begin{bmatrix} 0 & 0 & -1 \\ 1 & 0 & 0 \\ 0 & -1 & 0 \end{bmatrix} \cdot R_3^T(\alpha) \cdot [\text{SCS}] \\ [\text{ECI}] = \left\{ \begin{bmatrix} e_T & -e_N & -e_R \end{bmatrix} \cdot R_3^T(\alpha) \right\} \cdot [\text{SCS}] \end{cases}$$

$$\text{where} \begin{cases} \mathbf{e}_R = \dfrac{\boldsymbol{r}}{|\boldsymbol{r}|} \\ \mathbf{e}_N = \dfrac{\boldsymbol{r} \times \boldsymbol{v}}{|\boldsymbol{r} \times \boldsymbol{v}|} \\ \mathbf{e}_T = \mathbf{e}_N \times e_R \\ \alpha = -\psi \end{cases} \tag{4}$$

where $R_3(\cdot)$ denotes the rotation matrix about the third axis, which is the axis $\mathbf{Z_S}$ for the SCS. It should be noted that the roll and pitch angles of the yaw-attitude model still default to zero.

C. Effect of Attitude Error

Obviously, compared with the zero-attitude model, the yaw-attitude model contains different attitude errors. To verify the advantage of the yaw-attitude model over the zero-attitude model, it is necessary to derive relevant mathematical formulas to compare the different effects of these two model errors on ZY3-03 POD. These two models differ in whether the yaw angle is present or not. Previous studies have shown that the drift angle is typically less than ± 4 ° [25], indicating that the variation in the effective area of the satellite body caused by yaw-attitude should be less than 0.25% [1-cos(±4°)]. In addition, empirical accelerations and relevant dynamical coefficients are often estimated to compensate for the error of nonconservative forces in POD processing [32]. Theoretically, the differences in nonconservative forces caused by these two attitude models should be negligible. Therefore, the following text will only focus on analyzing the different effects of these two models on the transformation from APC to CoM, whose errors would be reflected in the final orbit results directly, and ignore their effects on nonconservative forces.

During the transformation from APC to CoM, the step related to the satellite attitude involves converting the offset vector between APC and CoM from SCS O_S–$\mathbf{X_S Y_S Z_S}$ into LOCS O_S–$\mathbf{RTN}$ or ECI O–$\mathbf{XYZ}$. To facilitate the analysis of transformation errors, according to Fig. 2, the transformation from SCS to LOCS is established as follows:

$$[\text{LOCS}] = \begin{bmatrix} 0 & 0 & -1 \\ 1 & 0 & 0 \\ 0 & -1 & 0 \end{bmatrix} \cdot \left\{ R_1^T(\gamma) R_2^T(\beta) R_3^T(\alpha) \right\} \cdot [\text{SCS}] \tag{5}$$

where α, β, and γ represent the yaw, pitch, and roll angles, respectively, $R_1(\cdot)$ and $R_2(\cdot)$ denote the rotation matrix about the second and third axes which represent the axes $\mathbf{X_S}$ and $\mathbf{Y_S}$ in the SCS, respectively. Based on (5), if the offset vector from APC to CoM under SCS is defined as $[\Delta X_S, \Delta Y_S, \Delta Z_S]$, using the actual attitude angles $(\alpha', \beta', \gamma')$, the actual transformed vector $[\Delta R', \Delta T', \Delta N']$ under LOCS could be expressed as follows:

$$\begin{cases} \Delta R' = \left(\cos\alpha' \sin\beta' \cos\gamma' - \sin\alpha' \sin\gamma'\right) \Delta X_S \\ - \left(\sin\alpha' \sin\beta' \cos\gamma' + \cos\alpha' \sin\gamma'\right) \Delta Y_S \\ - \cos\beta' \cos\gamma' \Delta Z_S \\ \Delta T' = \cos\alpha' \cos\beta' \Delta X_S - \sin\alpha' \cos\beta' \Delta Y_S + \sin\beta' \Delta Z_S \\ \Delta N' = -\left(\cos\alpha' \sin\beta' \sin\gamma' + \sin\alpha' \cos\gamma'\right) \Delta X_S \\ + \left(\sin\alpha' \sin\beta' \sin\gamma' - \cos\alpha' \cos\gamma'\right) \Delta Y_S \\ + \cos\beta' \sin\gamma' \Delta Z_S \end{cases}$$

$$\Rightarrow \begin{cases} \Delta R' \approx -\sin\alpha' \sin\gamma' \Delta X_S - \cos\alpha' \sin\gamma' \Delta Y_S \\ - \cos\gamma' \Delta Z_S \\ \Delta T' \approx \cos\alpha' \Delta X_S - \sin\alpha' \Delta Y_S \\ \Delta N' \approx -\sin\alpha' \cos\gamma' \Delta X_S - \cos\alpha' \cos\gamma' \Delta Y_S \\ + \sin\gamma' \Delta Z_S \end{cases}$$

$$\left(\text{special case I} : \beta' \approx 0°\right)$$

$$\Rightarrow \begin{cases} \Delta R' \approx -\Delta Z_S \\ \Delta T' \approx \cos\alpha' \Delta X_S - \sin\alpha' \Delta Y_S \\ \Delta N' \approx -\sin\alpha' \Delta X_S - \cos\alpha' \Delta Y_S \end{cases}$$

$$\left(\text{special case II} : \ \beta' \approx 0°, \gamma' \approx 0°\right). \tag{6}$$

In (6), two sets of approximate formulas are provided for two specific cases. The first applies when the pitch angle is approximately zero, while the second applies when both the pitch and roll angles are approximately zero. Similarly, according to (3) and (4), the transformed offset vectors $[\Delta R_{\text{zero}}, \Delta T_{\text{zero}}, \Delta N_{\text{zero}}]$ and $[\Delta R_{\text{yaw}}, \Delta T_{\text{yaw}}, \Delta N_{\text{yaw}}]$ based on the zero-attitude model and the yaw-attitude model could be obtained as follows:

$$\begin{cases} \begin{bmatrix} \Delta R_{\text{zero}} \\ \Delta T_{\text{zero}} \\ \Delta N_{\text{zero}} \end{bmatrix} = \begin{bmatrix} -\Delta Z_S \\ \Delta X_S \\ -\Delta Y_S \end{bmatrix}, \text{with } \alpha = 0, \beta = 0, \gamma = 0 \\ \begin{bmatrix} \Delta R_{\text{yaw}} \\ \Delta T_{\text{yaw}} \\ \Delta N_{\text{yaw}} \end{bmatrix} = \begin{bmatrix} -\Delta Z_S \\ \cos(-\psi) \Delta X_S - \sin(-\psi) \Delta Y_S \\ -\sin(-\psi) \Delta X_S - \cos(-\psi) \Delta Y_S \end{bmatrix} \\ \text{with } \alpha = -\psi, \beta = 0, \gamma = 0 \end{cases} \tag{7}$$

Using the actual offset vector $[\Delta R', \Delta T', \Delta N']$ in (6) as a reference, the errors in $[\Delta R_{\text{zero}}, \Delta T_{\text{zero}}, \Delta N_{\text{zero}}]$ and $[\Delta R_{\text{yaw}}, \Delta T_{\text{yaw}}, \Delta N_{\text{yaw}}]$can be directly calculated as follows:

$$\begin{cases} \begin{bmatrix} \delta R_{\text{zero}} \\ \delta T_{\text{zero}} \\ \delta N_{\text{zero}} \end{bmatrix} = \begin{bmatrix} \Delta R_{\text{zero}} - \Delta R' \\ \Delta T_{\text{zero}} - \Delta T' \\ \Delta N_{\text{zero}} - \Delta N' \end{bmatrix} = \begin{bmatrix} -\Delta Z_S - \Delta R' \\ \Delta X_S - \Delta T' \\ -\Delta Y_S - \Delta N' \end{bmatrix} \\ \begin{bmatrix} \delta R_{\text{yaw}} \\ \delta T_{\text{yaw}} \\ \delta N_{\text{yaw}} \end{bmatrix} = \begin{bmatrix} \Delta R_{\text{yaw}} - \Delta R' \\ \Delta T_{\text{yaw}} - \Delta T' \\ \Delta N_{\text{yaw}} - \Delta N' \end{bmatrix} \\ = \begin{bmatrix} -\Delta Z_S - \Delta R' \\ \cos(-\psi) \Delta X_S - \sin(-\psi) \Delta Y_S - \Delta T' \\ -\sin(-\psi) \Delta X_S - \cos(-\psi) \Delta Y_S - \Delta N' \end{bmatrix}. \end{cases} \tag{8}$$

The equation indicates that the transformation errors are related to not only the installation position of the GNSS receiver antenna but also the actual attitude variation for a particular satellite.

For the ZY3-03 satellite, the installation position $(\Delta X_S, \Delta Y_S, \Delta Z_S)$ of GPS antenna is about (+1232.20, +0.78, +1178.32) mm under SCS O_S–$\mathbf{X_S Y_S Z_S}$, where the offset component $\Delta Y_S = +0.78$mm is very close to zero. Moreover, it is imperative that the onboard Earth observation payload maintains a stable Earth-pointing direction most of the time to ensure accurate and stable measures. Typically, the actual roll and pitch angles (β', γ') of the satellite platform remain close to or even at zero for extended periods of time. Therefore, the computation of the actual offset vector $[\Delta R', \Delta T', \Delta N']$ complies with "special case II $(\beta' \approx 0°; \gamma' \approx 0°)$" of (6) for the majority of the time. Based on the premises $\Delta Y_S \approx 0.0$ and $(\beta' \approx 0°; \gamma' \approx 0°)$, the offset transformation errors for two attitude models in (8) can be expressed as follows:

$$\begin{cases} \begin{bmatrix} \delta R_{\text{zero}} \\ \delta T_{\text{zero}} \\ \delta N_{\text{zero}} \end{bmatrix} \approx \begin{bmatrix} 0 \\ \left(1-\cos\alpha'\right)\Delta X_S \\ \sin\alpha'\Delta X_S \end{bmatrix} \\ \begin{bmatrix} \delta R_{\text{yaw}} \\ \delta T_{\text{yaw}} \\ \delta N_{\text{yaw}} \end{bmatrix} \approx \begin{bmatrix} 0 \\ \left(\cos\left(-\psi\right)-\cos\alpha'\right)\Delta X_S \\ \left(\sin\alpha'-\sin\left(-\psi\right)\right)\Delta X_S \end{bmatrix}. \end{cases} \tag{9}$$

It is evident from (9) that the offset transformation errors in the R-direction are almost zero for both the attitude models. For the ZY3-03 satellite, the existence of the yaw angle is essentially to compensate for the drift angle in the opposite direction. Previous studies have shown that the drift angle ψ is typically less than ±4° [25], so the actual yaw angle α' close to the opposite of the drift angle theoretically, i.e., $\alpha' \approx -\psi$, should also vary at the range of ± 4° most of the time. Based on the premises $\alpha' \approx -\psi$ and $\alpha' \leq \pm 4°$, the maximum offset transformation errors for two attitude models in the T/N-directions can be obtained further as follows:

$$\begin{cases} |\delta T_{\text{zero}}| \approx \left|\left(1-\cos\alpha'\right)\Delta X_S\right| \leq \left(1-\cos 4°\right)|\Delta X_S| \\ \qquad\qquad \approx 3.0 \text{ mm} \\ |\delta N_{\text{zero}}| \approx \left|\sin\alpha'\Delta X_S\right| \leq \sin 4°\,|\Delta X_S| \approx 86.0 \text{ mm} \\ \left|\delta T_{\text{yaw}}\right| \approx \left|\left(\cos\left(-\psi\right)-\cos\alpha'\right)\Delta X_S\right| \approx 0.0 \text{ mm} \\ \left|\delta N_{\text{yaw}}\right| \approx \left|\left(\sin\alpha'-\sin\left(-\psi\right)\right)\Delta X_S\right| \approx 0.0 \text{ mm}. \end{cases} \tag{10}$$

It is evident from (10) that neglecting the yaw angle in the zero-attitude model results in significant offset transformation errors of several centimeters (8.6 cm) in the N-direction for the ZY3-03 satellite, but the offset transformation errors in the T-direction is less than 3.0 mm, which is small enough to be ignored. As for the yaw-attitude model, the offset transformation errors of the yaw-attitude model in the T/N-directions are all near zero. Therefore, it can be concluded that the yaw-attitude model provides a more precise description of the ZY3-03 satellite's yaw-steering state compared with the zero-attitude model, so this precision renders the transformation errors negligible most of the time for centimeter-level POD.

However, it is also important to consider some special situations concerning the satellite attitude. When the ZY3-03 satellite needs to observe some specific areas at certain times, the satellite platform may exhibit short-term, large-scale wide-angle side swing. At this time, the actual roll angle exhibits irregular variation and cannot be expressed by the analytical attitude model. The proposed yaw-attitude model, which assumes a roll angle of zero to compute the drift angle, may no longer depict the yaw-steering state accurately. In such a situation, the actual offset transformation from SCS to LOCS can only conform to the "special case I $\left(\beta' \approx 0°\right)$" of (6). Based on the premises $\beta' \approx 0°$ and $\Delta Y_S \approx 0.0$, the offset transformation errors should be expressed as follows:

$$\begin{cases} \begin{bmatrix} \delta R_{\text{zero}} \\ \delta T_{\text{zero}} \\ \delta N_{\text{zero}} \end{bmatrix} \approx \begin{bmatrix} \sin\alpha'\sin\gamma'\Delta X_S + \left(\cos\gamma'-1\right)\Delta Z_S \\ \left(1-\cos\alpha'\right)\Delta X_S \\ \sin\alpha'\cos\gamma'\Delta X_S - \sin\gamma'\Delta Z_S \end{bmatrix} \\ \begin{bmatrix} \delta R_{\text{yaw}} \\ \delta T_{\text{yaw}} \\ \delta N_{\text{yaw}} \end{bmatrix} \\ \approx \begin{bmatrix} \sin\alpha'\sin\gamma'\Delta X_S + \left(\cos\gamma'-1\right)\Delta Z_S \\ \left(\cos\left(-\psi\right)-\cos\alpha'\right)\Delta X_S \\ \left(\sin\alpha'\cos\gamma'-\sin\left(-\psi\right)\right)\Delta X_S - \sin\gamma'\Delta Z_S \end{bmatrix}. \end{cases} \tag{11}$$

Based on (11), it can be inferred that in this particular case, whether the zero-attitude model or the yaw-attitude one is used, significant offset transformation errors in the $R/T/N$-directions may be generated for the ZY3-03 satellite.

III. Experiments and Analysis

To demonstrate the effectiveness of the proposed yaw-attitude model, it is very crucial to conduct the attitude error analyses and the POD experiments based on the real data. The onboard GPS, SLR, and measured attitude data of the ZY3-03 satellite covering the period from 2020/244 to 2020/366 are collected for the experiments. It should be noted that the GPS data were unavailable for several days during this period due to data transmission failures or the loss of numerous observation records. Consequently, a usable dataset of 107 days is obtained. Regarding SLR data, only a limited number of SLR data points (201) from the SHA2 station are available for orbit validation, as the SLR data of ZY3-03 are not publicly accessible. Nonetheless, these data points suffice for the validation of orbit accuracy.

A. Solutions and Strategies

In the experiments, precise measured attitude data from the star sensor are used as references to compute the actual attitude angles $(\alpha', \beta', \gamma')$ of the satellite, then the transformation errors $[\delta R_{\text{zero}}, \delta T_{\text{zero}}, \delta N_{\text{zero}}]$ and $[\delta R_{\text{yaw}}, \delta T_{\text{yaw}}, \delta N_{\text{yaw}}]$ for the zero-attitude model and the yaw-attitude model could be computed and compared directly. Three solutions are generated to examine the different impacts of attitude models on POD. They are Solution I (measured attitude), Solution II (zero-attitude), and Solution III (yaw-attitude). The attitudes in Solutions II and III are computed using the zero-attitude model

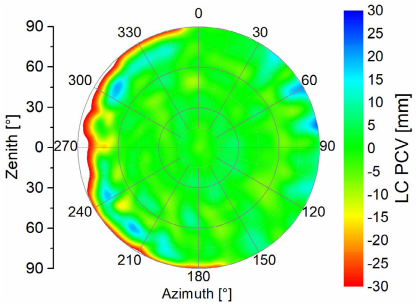

Fig. 3. Azimuth-zenith PCV map of GPS *LC*; the azimuth of 270° represents the flight direction.

and the proposed yaw-attitude model, respectively, whereas Solution I based on precise measured attitude data could generate the referent orbits to assess the orbit accuracy of Solutions II and III.

Apart from the differences in attitude models, three POD solutions share identical data processing strategies, as outlined in Table I. Dual-frequency carrier phase and pseudorange measurements of GPS L1/L2 are used to form ionosphere-free combinations (LC + PC). The precise ephemeris of GPS satellites released by the International GNSS Service (IGS) is used to calculate the precise orbits and clocks of the GPS satellites. The phase center offset (PCO) and phase center variation (PCV) of GPS satellites are corrected using the IGS-recommended model from "igs14.atx." The PCO values of the ZY3-03 satellite are provided by the satellite manufacturer, while the PCVs are estimated, whose distribution map is illustrated in Fig. 3. The dynamical models are set as complete and precise as possible, encompassing the gravity of the Earth, N-body gravitational perturbation, Earth and ocean tides, relativistic effects, solar and Earth radiation, atmospheric drag, etc. In Addition, empirical accelerations in the along-track and cross directions, and the atmospheric drag coefficient, are estimated as piecewise constants (PWC) to compensate for the error of modeled forces. Finally, all the parameters are estimated using the least square in batch mode.

B. Attitude Error Analysis

Fig. 4 displays the yaw, pitch, and roll angles of the ZY3-03 satellite obtained from the measured attitude, the zero-attitude model, and the yaw-attitude model on 2020/336, respectively. When the measured attitude is taken as the actual value, it can be observed clearly that the actual pitch and roll angles are in close proximity to zero and fluctuate within the range of $\pm 0.05°$ and $\pm 0.002°$, respectively, for vast majority of epochs. This indicates that it is reasonable to default the pitch and roll angles as zero for vast majority of the time in the yaw-attitude model. The actual yaw angle α' varies periodically within the range of $\pm 4°$. The yaw angle of the zero-attitude model is set as zero, while that of the yaw-attitude model exhibits a variation pattern and amplitude similar to the actual one α'. Fig. 5 illustrates the discrepancies between the computed yaw angle $-\psi$ by the yaw-attitude model and the actual one α'. As can be seen clearly, the yaw-attitude model has yaw angle errors of less than $\pm 0.01°$ for the majority of the time. Figs. 4 and 5 demonstrate fully that the yaw-attitude model could describe the yaw variation in the satellite more accurately most of the time compared with the zero-attitude model.

TABLE I
DETAILED STRATEGIES FOR POD EXPERIMENTS

Measurement model	
GPS observations	Dual-frequency ionosphere-free carrier phase (LC) and pseudorange (PC) measurements with the sampling interval of 10s
GPS orbit and clock	IGS final precise orbit and clock products
GPS PCO and PCV	PCO and PCV model from igs14.atx [26]
Receiver clock offset	An individual epoch-wise clock offset
Ambiguity	Real constant value for each ambiguity pass
Installation position of LEO GPS antenna	The offset of the antenna reference point (ARP) w.r.t the Center of Mass (CoM) is (+1232.20, +0.78, +1178.32)mm
PCO and PCV of LEO GPS antenna	L1/L2 PCOs are (+0.24,-1.67,0.00)mm and (0.00, 0.00, +19.40)mm, respectively, provided by the manufacturer, which refer to mean antenna phase center (MAPC) w.r.t the antenna reference point (ARP). LC PCV are estimated
POD arc length	30 hours for each POD arc, 6 hours overlap arc between adjacent arcs
Dynamical model	
Earth gravity field	EIGEN-6S (150×150) [27], including the time-varying part
N-body gravitation	Moon, Sun and other planets, JPL DE405 (position) [28]
Solid earth tide	IERS Conventions 2010 [29]
Earth pole tide	IERS Conventions 2010 [28]
Ocean tide	FES2004 [30]
Ocean pole tide	IERS Conventions 2010 [29]
Relativistic effects	IERS Conventions 2010 [29]
Atmosphere drag	DTM94 model (density) [31], macro model, piece-wise constant drag coefficients with 180 min intervals
Solar/Earth radiation	Macro model, the radiation pressure coefficients are fixed
Empirical acceleration	Piece-wise constant empirical acceleration [32] coefficients in the along-track and cross directions with 90min and 90min intervals, respectively
Reference frame	
Coordinate system	ITRF 2014
Precession/nutation	IAU 2006/IAU 2000R06 model
Earth rotation parameters	IERS final EOP products
Estimation	
Estimator	Least square
Mode	Batch processing

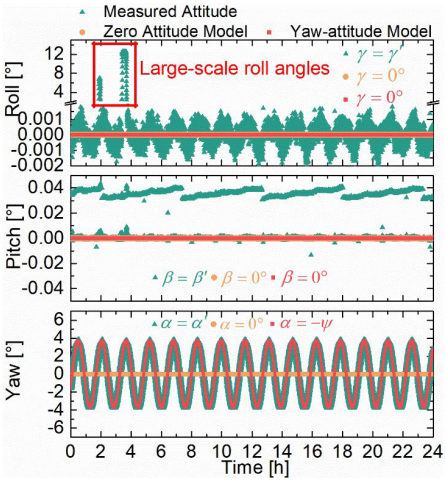

Fig. 4. Comparisons of yaw, pitch, and roll angles from measured attitude, zero-attitude model, and yaw-attitude model for the ZY3-03 satellite on 2020/336.

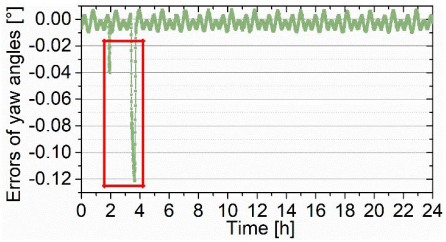

Fig. 5. Yaw angle errors of the yaw-attitude model using the yaw angle from measured attitude as reference for the ZY3-03 satellite on 2020/336.

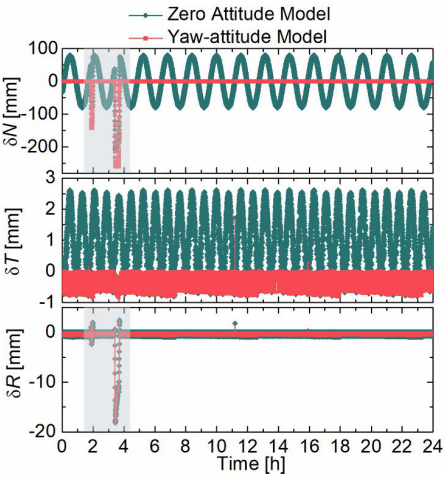

Fig. 6. Offset transformation errors in the *R/T/N*-directions from the zero-attitude model and yaw-attitude model for the ZY3-03 satellite on 2020/336.

The offset transformation errors $[\delta R_{\text{zero}}, \delta T_{\text{zero}}, \delta N_{\text{zero}}]$ and $[\delta R_{\text{yaw}}, \delta T_{\text{yaw}}, \delta N_{\text{yaw}}]$ for the zero-attitude and yaw-attitude model could be computed directly based on (6)–(8), as shown in Fig. 6. The transformations errors δR_{zero} and δR_{yaw} in the R-direction from these two models are near zero. The transformation errors from the zero-attitude model in the N-direction δN_{zero} are notable for the majority of the time, which vary periodically at a large range of $\pm$86mm, even though the transformation errors in the T-direction δT_{zero} is less than 3.0 mm. By comparison, those from the yaw-attitude model $(\delta T_{\text{yaw}}, \delta N_{\text{yaw}})$ are still near zero. The comparison demonstrates that the proposed yaw-attitude model can describe the variation in the yaw angle accurately in the majority of epochs, and then eliminate the offset transformation errors from APC to CoM in the T- and N-directions. This performance is consistent with the previous derivation based on (9) and (10).

Of course, the special situation cannot be ignored. As shown in the red rectangular area of Fig. 4, the actual roll angle reaches up to 8°–13° in some epochs over the period from 1 to 4 h, which is typically due to the satellite's wide-angle side swing when observing specific areas. Correspondingly, in these epochs, the difference between the calculated yaw angle and the actual one increases dramatically from $-0.01°$ to $-0.12°$, as shown in the red rectangular area of Fig. 5. In such a situation, notable transformation errors from APC to CoM are generated in the R/N-directions for both the models, as indicated by the gray shaded area of Fig. 6. This special performance in a few epochs also coincides with previous analysis based on (11).

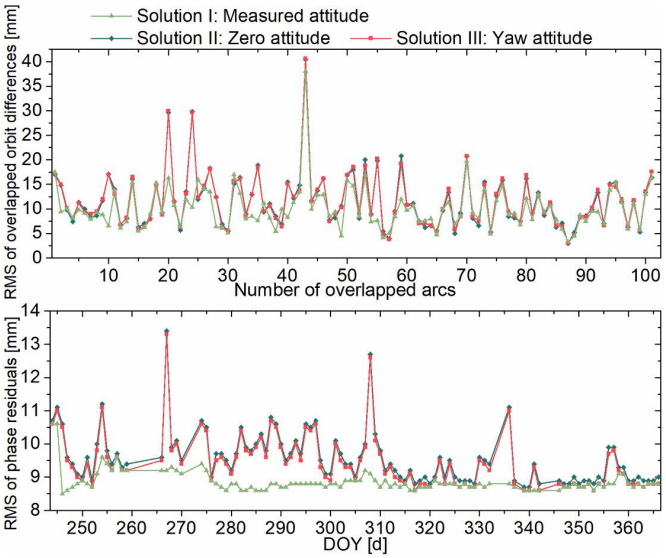

Fig. 7. Internal orbit consistency comparisons of three POD solutions; rms of overlapped orbit differences in 3-D position for each overlap arc (top) and rms of posterior *LC* phase residuals for each POD arc (bottom).

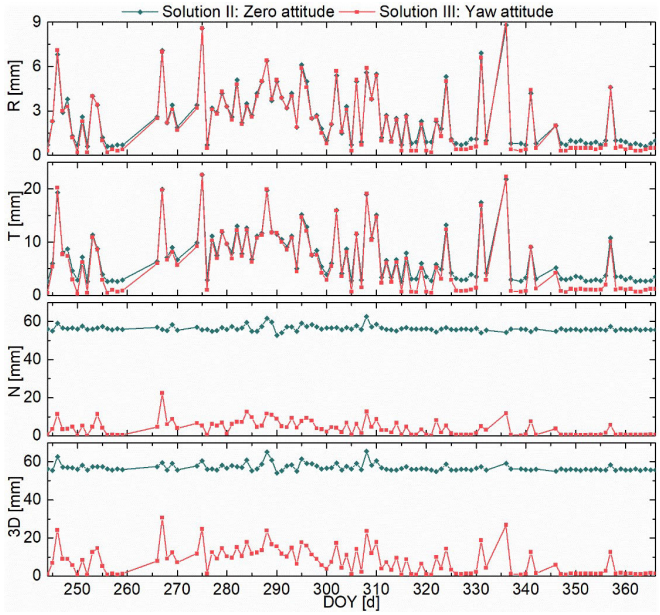

Fig. 8. RMS of daily orbit differences from referent orbits in the *R/T/N*-directions and 3-D position for Solutions II and III.

C. Orbit Accuracy Comparison

POD experiments are conducted to examine further the influence of transformation errors on the ultimate orbit outcomes for different attitude models. The accuracies of the orbits obtained from three solutions are compared using four criteria: overlapped orbit differences ("C1"), posterior phase residuals ("C2"), differences from referent orbits ("C3"), and validation residuals from SLR data ("C4"). The first two criteria evaluate the internal consistency of the orbit, while the latter two evaluate the external accuracy. Table II lists the overall performance comparison based on these four criteria. The second and third columns display the root-mean-square (rms) statistics of the R/T/N/3D orbit differences during the middle 5-h overlap arc [(0.5–5.5)h] between each pair of adjacent POD arcs, and the overall rms statistics of the

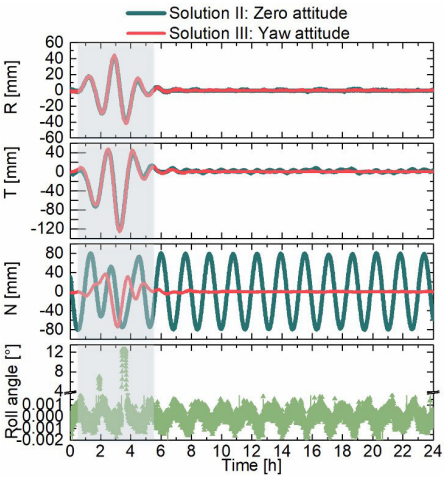

Fig. 9. Orbit error curves of Solution II-III in the *R/T/N*-directions on 2020/336; Variation curve of roll angle are listed in the bottom subgraph.

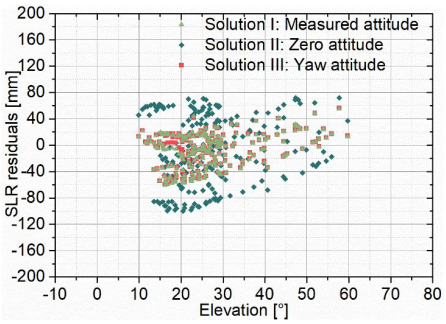

Fig. 10. Posterior residuals of SLR validation at different elevations for Solution I-III.

posterior LC phase residuals for all POD arcs, respectively. It can be observed clearly that the internal orbit consistencies of Solutions II and III are almost identical, and Solution I only exhibits slightly better performance than the other two. Fig. 7 also supports the almost identical internal orbit consistencies of Solutions II and III, as evidenced by the rms statistics of orbit differences for each overlap arc and the daily rms statistics of posterior phase residuals, respectively. It indicates an essential fact that the orbit errors caused by neglecting the yaw angle cannot be detected by the internal orbit consistency metric. The reason is quite understandable. First, the offset transformation errors caused by neglecting the yaw angle mainly manifests in the T/N-directions, while those in the R-direction are nearly zero. Therefore, the caused errors are difficult to manifest in the direction of the observation path, making it challenging to demonstrate through changes in the posterior phase residuals. Second, the overlapped orbit differences can only verify the consistency of the models used in two adjacent POD arcs. Thus, as long as a consistent model is uniformly adopted, whether it is a zero-attitude model or a yaw-attitude model, the differences in overlapping arcs may be all minimal. It also seems to be an important reason why the yaw-attitude for drift angle compensation is easily ignored by previous POD studies.

Unlike the internal orbit consistency, the negative impact of ignoring the yaw angle can be well-revealed in the evaluation of external orbit accuracy. Using the orbit results of Solution I as a reference, the overall rms statistics of the orbit differences

TABLE II
ORBIT ACCURACY COMPARISONS OF THREE SOLUTIONS WITH FOUR CRITERIA (C1: OVERLAPPED ORBIT DIFFERENCES; C2: POSTERIOR PHASE RESIDUALS; C3: DIFFERENCES FROM REFERENT ORBITS; C4: VALIDATION RESIDUALS FROM SLR DATA)

Solutions	Accuracy assessment criteria (unit: mm)			
	C1 R/T/N/3D RMS	C2 RMS	C3 R/T/N/3D RMS	C4 mean±std RMS
Solution I	4.9/9.6/2.4/11.0	8.9	/	-7.7±25.5 26.6
Solution II	5.5/10.8/4.4/12.9	9.6	3.1/8.6/56.3/57.0	-7.9±52.7 53.3
Solution III	5.5/10.9/4.4/12.9	9.5	3.1/8.2/5.5/10.3	-7.2±25.4 26.4

in the $R/T/N$-directions and 3-D position are listed in the fourth column of Table II. It is evident that the overall orbit accuracies of Solution II in the R/T-direction are almost identical to those of Solution III, but the orbit accuracy of Solution II in the N-direction is much lower than that of Solution III. Fig. 8 presents the daily rms of orbit differences in the $R/T/N$-directions and 3-D position for Solutions II and III further. It also shows clearly that the daily orbit accuracy of Solution III is much better than that of Solution II especially in the N-direction. This performance can be attributed to the zero-attitude model that neglects the yaw angle for compensating drift angle, resulting in a notable transformation error from APC to CoM in the N-direction, exactly as (10) and Fig. 6 indicate. Consequently, the transformed CoM deviates notably from the actual one in the N-direction due to this transformation error.

Fig. 9 illustrates the orbit error curves of Solutions II and III in the $R/T/N$-directions on 2020/336, providing a clearer view of the orbit errors in the N-direction caused by the negligence of the yaw angle. It can be observed that during the period from 5.5 to 24 h, the error curve of Solution III in the N-direction is near the zero axis, while that of Solution II varies periodically within a range of about ±86 mm. This error amplitude corresponds to the analysis results regarding the effects of attitude errors, as demonstrated in (10) and Fig. 6. In conclusion, Figs. 8 and 9 provide comprehensive evidence that disregarding the yaw angle in the zero-attitude model would result in notable periodical orbit errors in the N-direction for the ZY3-03 satellite. In other words, the proposed yaw-attitude model describes the yaw angle accurately, which can eliminate the orbit errors in the N-direction effectively. Of course, it is also worth noting that as indicated by the gray shaded area in Fig. 9, the orbit errors in the $R/T/N$-directions are all up to several centimeters for both Solutions II and III during the period from 0.5 to 5.5 h. The cause of this performance is clear that the roll angle of the ZY3-03 satellite reaches up to 8°–13° in a few epochs during this period, and neither the zero-attitude model nor the yaw-attitude model can express this irregular roll variation accurately. As a result, notable transformation errors from APC to CoM are generated in the $R/T/N$-directions for both the solutions, as just shown in (11) and Fig. 6.

The SLR validation further highlights the effectiveness of the yaw-attitude model for achieving higher precision orbit

determination. The overall mean, standard deviation (std), and rms statistics presented in the fifth column of Table II demonstrate that the external orbit accuracy of Solution III is almost equivalent to that of Solution I, and significantly better than that of Solution II. Fig. 10 displays SLR posterior residuals at different elevations for Solutions I–III. It is evident that the elevations of SLR measurements range from 10° to 60°, and SLR residuals for Solution II vary from −100 to 80 mm. In contrast, SLR residuals of Solution III decrease dramatically to the range of ±60 mm. This is because Solution II fails to consider the yaw-attitude of the ZY3-03 satellite, resulting in orbit errors in the N-direction that are projected onto the path of laser ranging, which causes notable SLR residuals. On the other hand, Solution III describes the yaw angle accurately, ensuring that no notable orbit errors in the N-direction exist. Importantly, the SLR residual distribution for Solution III is nearly identical to that of Solution I, except for a slight difference at low elevations from 10° to 20°. These performances demonstrate that higher precision POD can be achieved based on the proposed yaw-attitude model compared with the zero one.

IV. Summary and Conclusion

Many high-resolution remote sensing satellites represented by the ZY3-03 satellite maintain a special yaw-steering state to compensate for the drift angle of onboard TDICCD cameras. The commonly used zero-attitude model in GNSS-based POD of geodetic or telecommunication satellites usually assumes zero yaw, pitch, and roll angles and neglects the yaw variation in the satellite platform. We present a targeted yaw-attitude model to describe this special attitude variation in this contribution. Considering the fact that the purpose of yaw control is to compensate for the drift angle of onboard TDICCD cameras for remote sensing satellites, the proposed model calculates the drift angle based on the position and velocity of the LEO satellite first, and then uses the opposite of the drift angle as the yaw angle, even though it still defaults to zero roll and pitch angles.

Taking the ZY3-03 satellite as the research target, the analyses have demonstrated that the zero-yaw assumption in the zero-attitude model would lead to significant transformation errors from APC to CoM in the normal direction, while the proposed model could describe the actual yaw variation accurately, avoiding these transformation errors. The experiments have displayed clearly that the calculated yaw angle from the proposed model closely approximates the actual one, only with differences of less than ±0.01° most of the time. POD assessment results from various aspects have also shown that the adoption of the yaw-attitude model could eliminate the notable orbit errors in the normal direction caused by the zero-yaw assumption of the zero-attitude model in the majority of epochs, even though, like the zero-attitude model, it still cannot eliminate orbit errors caused by the large-scale side swing of the satellite in a few epochs. Furthermore, the results indicate that the POD accuracy based on the proposed model is much better than that based on the zero-attitude model and almost as good as that with the measured attitude data. Therefore, it can be concluded that the proposed yaw-attitude model is a significantly improved model for higher precision orbit determination of remote sensing satellites such as ZY3-03, especially in the absence of measured attitude data.

Acknowledgment

The authors are very grateful to the International GNSS Service (IGS) for providing the GPS precise orbit and clock products. Special thanks to the Shanghai Astronomical Observatory, Chinese Academy of Sciences, for providing the SLR data of the ZY3-03 satellite. The numerical calculations in this article have been done on the supercomputing system in the Supercomputing Center of Wuhan University.

References

[1] B. Fang and E. Seifert, "An evaluation of global positioning system data for Landsat-4 orbit determination," in *Proc. 23rd Aerosp. Sci. Meeting*, Reno, NV, USA, Jan. 1985, p. 286.

[2] C. Hwang, T.-P. Tseng, T. Lin, D. Švehla, and B. Schreiner, "Precise orbit determination for the FORMOSAT-3/COSMIC satellite mission using GPS," *J. Geodesy*, vol. 83, no. 5, pp. 477–489, May 2009.

[3] W. Bertiger et al., "Sub-centimeter precision orbit determination with GPS for ocean altimetry," *Mar. Geodesy*, vol. 33, no. 1, pp. 363–378, Aug. 2010.

[4] H. Bock et al., "GPS-derived orbits for the GOCE satellite," *J. Geodesy*, vol. 85, no. 11, pp. 807–818, May 2011.

[5] Y.-S. Li, C. Hwang, T.-P. Tseng, C.-Y. Huang, and H. Bock, "A near-real-time automatic orbit determination system for COSMIC and its follow-on satellite mission: Analysis of orbit and clock errors on radio occultation," *IEEE Trans. Geosci. Remote Sens.*, vol. 52, no. 6, pp. 3192–3203, Jun. 2014.

[6] J. van den IJssel, J. Encarnação, E. Doornbos, and P. Visser, "Precise science orbits for the swarm satellite constellation," *Adv. Space Res.*, vol. 56, no. 6, pp. 1042–1055, Sep. 2015.

[7] M. Li et al., "Precise orbit determination of the Fengyun-3C satellite using onboard GPS and BDS observations," *J. Geodesy*, vol. 91, no. 11, pp. 1313–1327, Apr. 2017.

[8] L. Wang et al., "Centimeter-level precise orbit determination for the Luojia-1A satellite using BeiDou observations," *Remote Sens.*, vol. 12, no. 12, p. 2063, Jun. 2020.

[9] O. Montenbruck, S. Hackel, M. Wermuth, and F. Zangerl, "Sentinel-6A precise orbit determination using a combined GPS/Galileo receiver," *J. Geodesy*, vol. 95, no. 9, p. 109, Sep. 2021.

[10] B. E. Schutz, B. D. Tapley, P. A. M. Abusali, and H. J. Rim, "Dynamic orbit determination using GPS measurements from TOPEX/POSEIDON," *Geophys. Res. Lett.*, vol. 21, no. 19, pp. 2179–2182, Sep. 1994.

[11] O. Montenbruck et al., "Tracking and orbit determination performance of the GRAS instrument on MetOp-A," *GPS Solutions*, vol. 12, no. 4, pp. 289–299, Apr. 2008.

[12] L. Cerri et al., "Precision orbit determination standards for the Jason series of altimeter missions," *Mar. Geodesy*, vol. 33, pp. 379–418, Aug. 2010.

[13] J. Yuan, C. Zhao, and Q. Wu, "Phase center offset and phase center variation estimation in-flight for ZY-3 01 and ZY-3 02 space-borne GPS antennas and the influence on precision orbit determination," in Chinese, *Acta Geodaetica et Cartographica Sinica*, vol. 47, no. 5, pp. 672–682, May 2018.

[14] Z. Kang, B. Tapley, S. Bettadpur, J. Ries, P. Nagel, and R. Pastor, "Precise orbit determination for the GRACE mission using only GPS data," *J. Geodesy*, vol. 80, no. 6, pp. 322–331, Jul. 2006.

[15] T.-P. Tseng, C. Hwang, and S. K. Yang, "Assessing attitude error of FORMOSAT-3/COSMIC satellites and its impact on orbit determination," *Adv. Space Res.*, vol. 49, no. 9, pp. 1301–1312, May 2012.

[16] W. Li, C. Hu, L. Zhang, and C. Yan, "Drift angle compensation method for a high-resolution and wide-range space camera," *Measurement*, vol. 158, Jul. 2020, Art. no. 107710.

[17] T. Yu, S. Xu, C. Han, Y. Li, and Y. Wang, "Batch-type real-time adjustment for drift angle of space camera," (in Chinese), *Opt. Precis. Eng.*, vol. 17, no. 8, pp. 1908–1914, Aug. 2009.

[18] Y. Sun, F. Yan, D. Xue, X. Wang, and X. Zhang, "Drift angle distribution and image quality decreasing of solar synchronizing elliptic orbit," (in Chinese), *Infr. Laser Eng.*, vol. 42, no. 3, pp. 767–773, 2013.
[19] Y. Wu, Y. Zhang, S. Han, L. Jin, and W. Wang, "Image motion compensation and MTF analyse of long array TDICCD space camera," (in Chinese), *Electron. Meas. Technol.*, vol. 37, no. 10, pp. 71–75, 2014.
[20] S. Gu, Y. Yan, K. Xu, and G. Jin, "Design of motion compensation mechanism of satellite remote sensing camera," *Proc. SPIE*, vol. 8196, pp. 587–594, Aug. 2011.
[21] K. Xu, G. Jin, S. Gu, Y. Yan, and Z. Sun, "Design of motion adjusting system for space camera based on ultrasonic motor," *Proc. SPIE*, vol. 8196, pp. 614–620, Aug. 2011.
[22] M. Huang, Y. Ge, F. Yang, and Q. Huang, "Analysis on image motion velocity and drift angle for agile satellite," (in Chinese), *Spacecraft Eng.*, vol. 24, no. 3, pp. 34–39, Jun. 2015.
[23] S. Ren, X. Fan, F. Zhang, and Z. Su, "Analysis of drift adjustment by a space optical camera platform," (in Chinese), *J. Spacecraft TT C Technol.*, vol. 36, no. 4, pp. 281–286, Aug. 2017.
[24] X. Tang et al., "The China ZY3–03 mission: Surveying and mapping technology for high-resolution remote sensing satellites," *IEEE Geosci. Remote Sens. Mag.*, vol. 8, no. 3, pp. 8–17, Sep. 2020.
[25] Q. Jing, "Research on computation model of bias angle for agile satellite," (in Chinese), *Spacecraft Eng.*, vol. 21, no. 4, pp. 16–20, Aug. 2012.
[26] P. Rebischung and R. Schmid, "IGS14/igs14. atx: A new framework for the IGS products," in *Proc. AGU Fall Meeting*, Vienna, Austria, 2016.
[27] C. Förste et al., "EIGEN-6: A new combined global gravity field model including GOCE data from the collaboration of GFZ Potsdam and GRGS Toulouse," in *Proc. EGU General Assembly*, Vienna, Austria, 2012, p. 2821.
[28] L. V. Morrison and D. W. Evans, "Check on JPL DE405 using modern optical observations," *Astron. Astrophys. Suppl. Ser.*, vol. 132, no. 3, pp. 381–386, May 1998.
[29] G. Petit and B. Luzum, "IERS conventions," Verlag des Bundesamts fur Kartographie und Geodasie, Frankfurt, Germany, IERS Tech. Note 36, 2010.
[30] F. Lyard, F. Lefevre, T. Letellier, and O. Francis, "Modelling the global ocean tides: Modern insights from FES2004," *Ocean Dyn.*, vol. 56, nos. 5–6, pp. 394–415, Dec. 2006.
[31] C. Berger, R. Biancale, F. Barlier, and M. Ill, "Improvement of the empirical thermospheric model DTM: DTM94—A comparative review of various temporal variations and prospects in space geodesy applications," *J. Geodesy*, vol. 72, no. 3, pp. 161–178, Mar. 1998.
[32] A. Jäggi, "Pseudo-stochastic orbit modeling of low Earth satellites using the Global Positioning System," Ph.D. thesis, Univ. Bern, Astronomical Inst., Bern, Switzerland, 2007.

Xuewen Gong received the B.S., M.S., and Ph.D. degrees from Wuhan University, Wuhan, China, in 2012, 2015, and 2020, respectively.

He is now working with the National Time Service Center, Chinese Academy of Sciences, Beijing, China, as an Associate Professor. His main research interests include precise orbit determination, autonomous navigation, and integrated precise orbit determination of GNSS/low Earth orbits (LEO) satellites.

Wanke Liu received the B.Sc., M.Sc., and Ph.D. degrees in geodesy and engineering surveying from the School of Geodesy and Geomatics, Wuhan University, Wuhan, China, in 2001, 2004, and 2008, respectively.

He is currently a Professor with Wuhan University. His main research interests include orbit determination of navigation satellites, precise positioning technology of GNSS, and low-cost multisensor integration technology.

Fuhong Wang received the Ph.D. degree in geodesy and engineering surveying from the School of Geodesy and Geomatics, Wuhan University, Wuhan, China, in 2006.

He is currently a Professor with Wuhan University. His current research focuses on satellite navigation and satellite orbit determination.

Qingpeng Li received the M.Sc. and Ph.D. degrees from Beijing Institute of Graphic Communication and China Academy of Space Technology, Beijing, China, in 2004 and 2011, respectively.

He is currently working as a Senior Engineer with China Center for Resources Satellite Data and Application, Beijing, China. His research interests include spacecraft design and satellite remote sensing data processing.

Jingmei Li received the B.S. and M.S. degrees from Wuhan University, Wuhan, China, in 2005 and 2007, respectively, and the Ph.D. degree from Aerospace Information Research Institute, Chinese Academy of Sciences, Beijing, China, in 2017.

She is currently a Senior Engineer with the Aerospace Information Research Institute, Chinese Academy of Sciences. She is mainly working on spaceborne LiDAR calibration and preprocessing and airborne image geometry correction processing.

Xueli Chang received the B.S. degree in geographical information system from Huazhong Agricultural University, Wuhan, China, in 2006, and the M.S. degree in cartography and geographic information systems and the Ph.D. degree in photogrammetry and remote sensing from Wuhan University, Wuhan, in 2009 and 2015, respectively.

He is currently an Associate Professor with the School of Computer Science, Hubei University of Technology, Wuhan. His research mainly focuses on high-resolution satellite data processing and quality improvement.

Shuaihe Gao received the Ph.D. degree from Harbin Engineering University, Harbin, China, in 2012.

He is a Professor with the National Time Service Center, Chinese Academy of Sciences, Beijing, China. He is mainly working on satellite navigation, satellite communication, and spatial time–frequency technology.